

Divergence angle consideration in energy spread measurement for high-quality relativistic electron beam in LWFA

Guang-Wei Lu(卢光伟), Yao-Jun Li(李曜均), Xi-Chen Hu(胡曦辰), Si-Yu Chen(陈思宇), Hao Xu(徐豪), Ming-Yang Zhu(祝铭阳), Wen-Chao Yan(闫文超), and Li-Ming Chen(陈黎明)

Citation: Chin. Phys. B, 2024, 33 (**6**): 064101. DOI: 10.1088/1674-1056/ad2dcb
Journal homepage: http://cpb.iphy.ac.cn; http://iopscience.iop.org/cpb

What follows is a list of articles you may be interested in

Effect of sharp vacuum-plasma boundary on the electron injection and acceleration in a few-cycle laser driven wakefield

Guo-Bo Zhang(张国博), Song Liu(刘松), De-Bin Zou(邹德滨), Ye Cui(崔野), Jian-Peng Liu(刘建鹏), Xiao-Hu Yang(杨晓虎), Yan-Yun Ma(马燕云), and Fu-Qiu Shao(邵福球)

Chin. Phys. B, 2023, 32 (**9**): 095202. DOI: 10.1088/1674-1056/acdc0c

Plasma density transition-based electron injection in laser wake field acceleration driven by a flying focus laser

Pan-Fei Geng(耿盼飞), Min Chen(陈民), Xiang-Yan An(安相炎), Wei-Yuan Liu(刘维媛), Xin-Zhe Zhu(祝昕哲), Jian-Long Li(李建龙), Bo-Yuan Li(李博原), and Zheng-Ming Sheng(盛政明)

Chin. Phys. B, 2023, 32 (**4**): 044101. DOI: 10.1088/1674-1056/acae79

Ion-focused propagation of a relativistic electron beam in the self-generated plasma in atmosphere

Jian-Hong Hao(郝建红), Bi-Xi Xue(薛碧曦), Qiang Zhao(赵强), Fang Zhang(张芳), Jie-Qing Fan(范杰清), and Zhi-Wei Dong(董志伟)

Chin. Phys. B, 2022, 31 (**6**): 064101. DOI: 10.1088/1674-1056/ac4a60

Physical properties of relativistic electron beam during long-range propagation in space plasma environment

Bi-Xi Xue(薛碧曦), Jian-Hong Hao(郝建红), Qiang Zhao(赵强), Fang Zhang(张芳), Jie-Qing Fan(范杰清), and Zhi-Wei Dong(董志伟)

Chin. Phys. B, 2021, 30 (**10**): 104103. DOI: 10.1088/1674-1056/ac192f

HEM_{11} mode magnetically insulated transmission[2mm] line oscillator: simulation and experiment

Wang Dong (王冬), Qin Fen (秦奋), Wen Jie (文杰), Chen Dai-Bing (陈代兵), Jin Xiao (金晓), An Hai-Shi (安海狮), Zhang Xin-Kai (张新凯)

Chin. Phys. B, 2012, 21 (**8**): 084101. DOI: 10.1088/1674-1056/21/8/084101

Divergence angle consideration in energy spread measurement for high-quality relativistic electron beam in laser wakefield acceleration

Guang-Wei Lu(卢光伟)[1], Yao-Jun Li(李曜均)[1], Xi-Chen Hu(胡曦辰)[1], Si-Yu Chen(陈思宇)[1], Hao Xu(徐豪)[1], Ming-Yang Zhu(祝铭阳)[1], Wen-Chao Yan(闫文超)[1,2,†], and Li-Ming Chen(陈黎明)[1,2,‡]

[1] *Key Laboratory for Laser Plasmas of Ministry of Education, Shanghai Jiao Tong University, Shanghai* 200240, *China*
[2] *IFSA Collaborative Innovation Center, Shanghai Jiao Tong University, Shanghai* 200240, *China*

(Received 24 November 2023; revised manuscript received 26 December 2023; accepted manuscript online 28 February 2024)

The thorough exploration of the transverse quality represented by divergence angle has been lacking yet in the energy spread measurement of the relativistic electron beam for laser wakefield acceleration (LWFA). In this work, we fill this gap by numerical simulations based on the experimental data, which indicate that in a C-shape magnet, magnetic field possesses the beam focusing effect, considering that the divergence angle will result in an increase in the full width at half maxima (FWHM) of the electron density distribution in a uniformly isotropic manner, while the length-to-width ratio decreases. This indicates that the energy spread obtained from the electron deflection distance is smaller than the actual value, regardless of the divergence angle. A promising and efficient way to accurately correct the value is presented by considering the divergence angle (for instance, for an electron beam with a length-to-width ratio of 1.12, the energy spread correct from 1.2% to 1.5%), providing a reference for developing the high-quality electron beam source.

Keywords: relativistic electron beams, acceleration by laser–plasma interactions, finite element analysis

PACS: 41.75.Ht, 52.38.Kd, 02.70.Dh **DOI:** 10.1088/1674-1056/ad2dcb

1. Introduction

High energy electron beams are widely used to produce ultraviolet light, high-energy x-rays, and gamma rays in large scientific facilities such as synchrotron radiation sources and free electron lasers. These beams play an important role in revealing electron dynamics, detecting biological molecule structures, and recording chemical reaction processes in many research fields.[1] The quality of the electron beam can be evaluated by the electron charge (Q), pulse width (Δt), energy spread (E_S), and so on.[2,3]

With the development of laser technology, significant breakthroughs have been made in laser wakefield acceleration (LWFA),[4–7] providing extremely high acceleration gradient.[8] In order to achieve the quality of electron beam equivalent to that of conventional accelerators, a lower E_S is required, under the constraint of the Q being limited by the beam loading effect.[1]

The energy spread is defined as the ratio of the energy width at half maximum of the energy spectrum (δE) to the energy at the peak[10] ($E_S = (\delta E/E_{max}) \times 100\%$). Researchers are committed to pursuing lower energy spread in theory[10–12] and in experiment.[3,13–23]

As a consequence, precise measurement of energy spread becomes particularly important. The usual method is to deflect the accelerated electron beam by using a stable magnetic field. Due to the relation between the Lorentz force and velocity, particles with different speeds (i.e., different energy values) experience different deflection forces and curvature radii. The particles eventually reside on different positions on the receiving screen where an image plate (IP) is placed,[23,24] and the deflection distances can be used to infer the particle velocities. For an electron beam, the FWHM of the electron density distribution on the receiving screen can be used to characterize the energy spread.[1] However, the above approach does not consider the transverse momentum due to the divergence angle θ, which has a direct effect on the final deflection distance of the electron.

In this work, we discuss the effect of the divergence angle on the energy spread, obtained by numerical simulations through using finite element methods based on experimental data. The qualitative influence of the energy spread measurements is investigated. By considering the inhomogeneity of the magnetic field and comparing two cases (with and without the divergence angle). The numerical simulation is based on COMSOL Multiphysics.[25]

2. Model

Based on the experimental results, we developed a complete model and used COMSOL Multiphysics to simulate the complete flight path of the electron beam from entering the magnet to being received by the detector. The simulation box size is set to 20 cm×20 cm×39.8 cm, and the magnetic field area is 2 cm×8 cm×16 cm. The simulation box is partitioned

†Corresponding author. E-mail: wenchaoyan@sjtu.edu.cn
‡Corresponding author. E-mail: lmchen@sjtu.edu.cn

© 2024 Chinese Physical Society and IOP Publishing Ltd

into 53164 tetrahedral meshes using a finite element algorithm with adaptive partitioning as shown in Fig. 1(a).

A total of 3×10^5 electrons are set to be in the electron beam and the initial propagation direction is along the positive z axis. According to the experimental data, the transversal density distribution of the incoming electron beams is assumed to be a two-dimensional Gaussian distribution. Its full width at half maximum (FWHM) in the x direction (x_{FWHM}) is 3.82 mm, and full width at half maxima in the y direction (y_{FWHM}) is 4.34 mm, with their ratio being 1.136. It is attributed to the divergence of angle and size of the electron beam moving from the source to the magnetic field region.

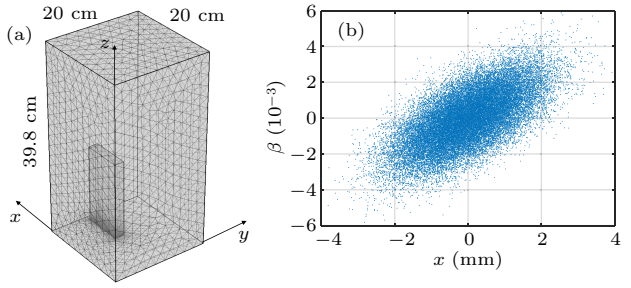


Fig. 1. (a) Three-dimensional model of experimental setup after adaptive meshing. (b) Distribution of transverse phase space ($\beta = v_x/v_z$) along x direction in incident plane in magnetic field region.

The energy distribution of the electron beam is set to a Gaussian distribution. In general, the energy spectrum can be fitted to a linear combination of multiple Gaussian distributions by using the algorithm given in Ref. [26]. The central energy of the electron beam is 150 MeV, the simulation time scale is set to 1.4 ns in time steps of 1 ps and the coordinates of all electrons can output at each time step.

In the phase space, the divergence angle is characterized by setting the transverse momentum distribution in the incident plane.[27] Starting from an initial point source, due to the presence of the divergence angle, the electron bunch with different transverse momentum components will gradually disperse.

As shown in Fig. 1(b), the mean of the particle velocity ratio ($\beta = v_x/v_z$) distribution in the positive direction of the x-axis coordinate is also positive, which is consistent with the above physical picture.[27] In a real situation, the transverse velocity component is very small compared with the longitudinal velocity component. Thus, according to $\beta = v_x/v_z = \tan(\theta) \approx \theta$ (the approximation is satisfied when the angle is very tiny), the divergence angle can be set to be the FWHM of β distribution. This setting leads to better robustness in particle simulation dynamic simulations.[28]

In contrast to conventional accelerators which uses quadrupole triplets to focus the electron beam, the divergence angle constitutes to be the key parameter for assessing LWFA. Therefore, no pre-treatment is applied prior to the magnet. The electron beam is incident from the center of the magnet entrance surface and deflected along the negative y axis as it passes through the magnet. Eventually, it resides on the detector at the top of the simulation box. Therefore, the top of the simulation box is assumed to be taken as a frozen boundary condition.

After completing the basic setup, the simulation program is run to obtain the motion trajectory of each electron as shown in Fig. 2. The numerical simulations yield an output x and y coordinate of the particles, and the scatter density analysis is performed by using the 'ksdensity' algorithm, which is widely used in statistics, machine learning, and other fields.[29,30] As shown in Fig. 2(d), the FWHM of the density distribution curves,[31] x_{FWHM} and y_{FWHM}, respectively represent the x size and y size of the deflected electron beam spot.

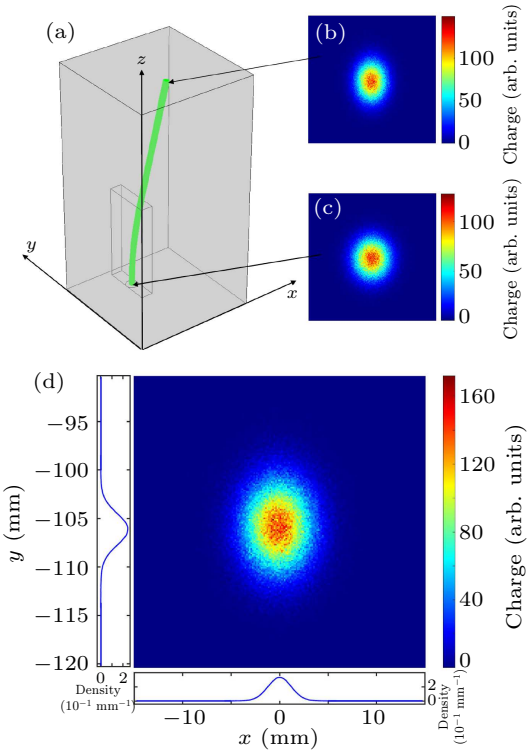


Fig. 2. (a) Trajectory of electron beam, (b) outgoing, (c) incident electron beam spots, (d) data processing using MATLAB, with color indicating the number of electrons in pixel and electric charge being in atomic units.

When the electron beam's pointing stability is less than 5 mrad, there is no discernible influence on the results within the precision threshold of 0.1 μm. When the incident deflection angle is large, the incidence deflection angle can be measured by IP in front of the magnet, and the average deflection angle can be used for numerical simulation.

3. Uniform magnetic field

For ease of comparison and validation, the magnetic field is initially set to 1-T field. Although the divergence angle cannot be zero in reality, the divergence angle is set to 0 in the numerical simulation in order to reflect the bias caused by the case where the divergence angle is not considered. Considering the experimental requirements, more points in a range

from 1% to 2% are taken to obtain the x_{FWHM} and y_{FWHM} of the electron distribution as shown in Fig. 3(a).

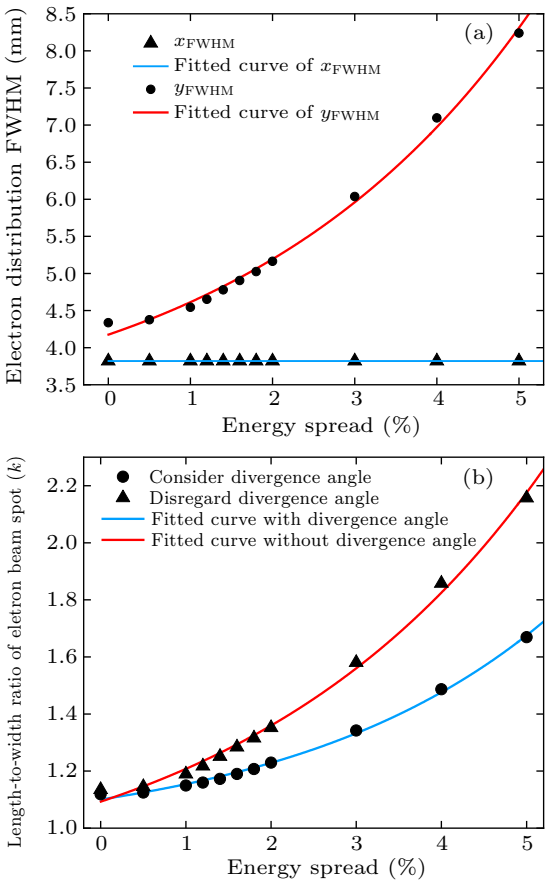


Fig. 3. Relationship between energy spread and FWHM of electronic density profile in the x direction and y direction on the detector surface (a) under a uniform magnetic field, irrespective of the divergence angle, and (b) under different divergence angles.

It can be found that the x_{FWHM} remains essentially constant, which is consistent with the physical picture that a magnetic field in the positive x direction does not produce a Lorentz force on the x component of the velocity. In addition, since the x_{FWHM} remains basically unchanged, we mainly use the aspect ratio of the two, namely the length-to-width ratio ($k = y_{\mathrm{FWHM}}/x_{\mathrm{FWHM}}$). It should be noted that for electron beams with the same center energy but different energy spreads, the x_{FWHM} remains constant due to the absence of the Lorentz force in the x direction. Therefore, k is a good physical quantity to calculate the energy spread of an electron bunch. As the energy spread increases, so does y_{FWHM}, showing an exponential growth trend, which indicates that the profile is stretched and the degree of elliptical flattening is greater. It is consistent that when the energy spread is large, the momentum variance increases, and the distance variance after being deflected by the magnetic field increases.

The divergence angle is set to 3.5 mrad based on experimental data. The data obtained are given in Table 1.

First, when the divergence angle is ignored, the k remains unchanged, still keeping the initial value. This is consistent with the fact that a monoenergetic electron beam is deflected in a uniform magnetic field without changing its spatial distribution. It can be seen that the introduction of a divergence angle leads to an increase in the FWHM, which is due to the fact that the distribution is broadened. It increases by 605.4 μm in the x direction and 616.0 μm in the y direction. It can be said that both increase uniformly. This is also consistent with the isotropy of the divergence angle in the transverse plane.

Table 1. Different divergence angle cases corresponding to FWHM data at zero energy divergence under uniform magnetic field, irrespective of divergence angle.

Divergence angle	x_{FWHM} (μm)	y_{FWHM} (μm)	k
Disregard divergence angle	3820.0	4335.6	1.1350
Consider divergence angle	4425.4	4951.6	1.1189

Then, we plot the comparison graph for k with and without the divergence angle. Since x and y increase equally and the ratio is a fraction greater than one, the aspect ratio in the case with divergence angle is less than in the case without divergence angle. In general, the divergence angle will have a suppression effect on the elliptical flattening of ellipse by the energy spread. For a simplified energy spread calculation without consideration the beam size (only the distance along the y axis is used), the suppression effect induced by the divergence angle can be subtracted through the above calculation.

4. Magnetic field of C-shaped magnet

In practice, we usually use a C-shaped magnet with a relatively uniform magnetic field in the center of its internal region. Based on actual measurements and calibration, data of the magnetic induction intensity (B) at different positions can be obtained and fitted. According to the characteristic of the C-shaped magnet, the B in the x direction can be considered to be constant. The fitting function and parameters are as follows:

$$B = B_{\max} \times \exp\left(-\frac{(z-0.08)^6}{m_{pz}}\right) \times \exp\left(-\frac{y^4}{m_{py}}\right),$$

where $B_{\max}$ represents the extreme value of magnetic induction intensity of the magnetic field, and it is 1.01 T, m_{pz} and m_{py} represent the degree of change of B in the z direction and y direction.

The inhomogeneity of the magnetic field leads to a narrowing of the y_{FWHM}. This is due to the fact that the magnetic field distribution also exhibits a peak in the middle and low on both sides, which leads to a lens-like focusing effect of the electron beam. As shown in Fig. 4, this focusing effect can reduce the y_{FWHM} while having no effect on the x_{FWHM}, causing the radio k to decrease. Moreover, the peak shifts towards

the negative y axis. This shift is mainly because the peak of the particle number density and the magnetic field are both located at the zero-point coordinate, which causes the particles at the peak to have a larger offset than those at the waist of the beam. Quantitatively, we can compare the data in Table 2 with those in Table 1. Without considering divergence angle, y_{FWHM} decreases from 4335.6 μm to 4083.4 μm.

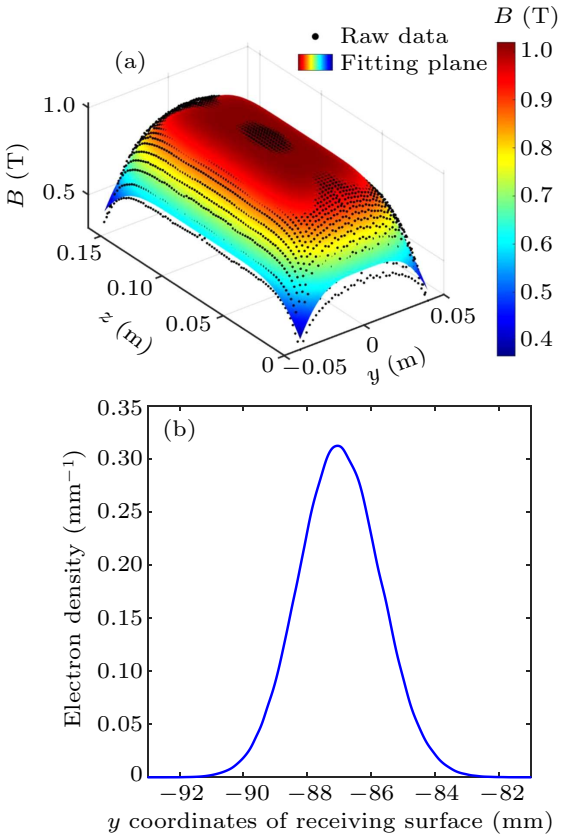


Fig. 4. (a) Magnetic field measured in the center plane ($x = 0.01$ m), with color representing the magnitude of the fit and points denoting sampled data. (b) Electron density distribution received by the detector plane at 0 energy spread, irrespective of the divergence angle, with the peak shifting to the negative y axis.

Table 2. Different divergence angle cases corresponding to FWHM data at zero energy divergence under magnetic field produced by C-shaped magnet.

Divergence angle	x_{FWHM} (μm)	y_{FWHM} (μm)	k
Disregard divergence angle	3820.0	4083.4	1.0690
Consider divergence angle	4429.1	4689.1	1.0587

The final discussion concerns the deflection of an electron beam in an inhomogeneous magnetic field with a divergence angle, which is very close to a real situation. Moreover, comparison simulations show that space charge effects do not obviously affect the results (within the precision threshold of 1 μm), and the computational scale is increased by a factor of 5, which is reasonable for pC electrons in a beam spot size of the nm scale. According to Table 2, x_{FWHM} and y_{FWHM} increase by 609.1 μm and 605.7 μm respectively. Since the magnetic field is in the x direction, only the y-axis component of the momentum has an effect in the z direction, which is negligible in a relativistic electron beam. In addition, the magnetic field produced by the C-shaped magnet exhibits symmetry, so that the effect of the divergence angle on the FWHM remains the same in both the x direction and the y direction.

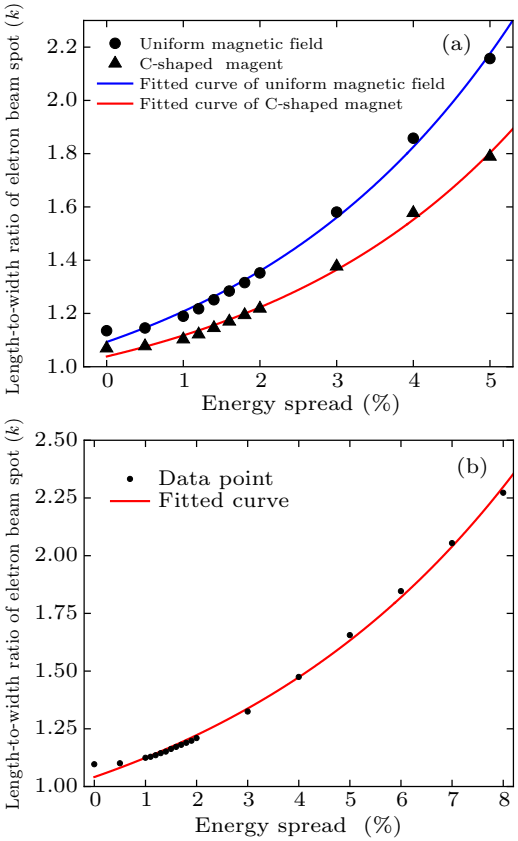


Fig. 5. Relationship between electron beam spot length-to-width radio k and the energy spread under uniform magnetic field produced by C-shaped magnet conditions, without (a) and with considering divergence angle.

As shown in Fig. 5(a), it can be observed that the overall k is smaller than that in the case of uniform magnetic field, reflecting the narrowing effect of the inhomogeneous magnetic field. The data show a good correlation and by fitting the data with two curves through using the exponential function as a reference, we obtain two curves:

$$k = 0.605 \times \mathrm{e}^{0.162E_{\mathrm{s}}} + 0.399$$

(without considering divergence angle),

$$k = 0.484 \times \mathrm{e}^{0.162E_{\mathrm{s}}} + 0.517,$$

(with considering divergence angle).

The two curves obtained exhibit highly consistent variations in the exponent factor. Therefore, the divergence angle is further studied as a variable, resulting in the following table where the goodness of fit (mathematically representing the degree of fitting between the regression curve and scattered values: the closer the exponent factor is to 1, the better the fitting degree is) is all greater than 0.99.

As indicated in Table 3, the fit is performed in the form of $k = A \cdot \exp(B \cdot E_s) + C$, where A denotes the coefficient of the exponential term reflecting the magnitude of the energy spread effect, B is the exponent factor of E_s, and C is the constant term corresponding to the influence of the divergence angle.

Table 3. In magnetic field produced by C-shaped magnet, the curve fitting of k varies with energy spread corresponding to different divergence angles. The corresponding parameter table is obtained by fitting in the form of $k = A \cdot \exp(B \cdot E_s) + C$.

Divergence angle (mrad)	A	B	C
0	0.605	0.162	0.399
2	0.554	0.162	0.458
3	0.508	0.162	0.501
3.5	0.484	0.162	0.517
4	0.459	0.162	0.547

It can be observed that the constant term (C) increases as the divergence angle increases, while the coefficient of the exponential term (A) gradually decreases. A larger divergence angle leads $r\,x_{\mathrm{FWHM}}$ and y_{FWHM} to increase, making the effect of E_s on the broadening in the y direction turn less significant. At different divergence angles, the trend of the variation in k follows the same exponential parameter (i.e., $\exp(0.162E_s)$), indicating that the divergence angle and E_s do not affect each other in terms of k. Furthermore, the fact that the influence of the divergence angle is reflected as a constant term also implies the invariant influence of the divergence angle on k across different energy spreads.

In experiment, the high-quality relativistic electron beam obtained via the LWFA mechanism is guided through a C-shaped magnet and directed onto a receiving screen. By calculating x_{FWHM} and y_{FWHM}, the length-to-width radio k is 1.12 as indicated in Fig. 6(a), and the back-calculated energy spread is 1.2% regardless of the divergence angle. Whereas, the energy spread is corrected to 1.5% by considering the divergence angle according to the data point in Fig. 5(b). Similarly, for the k value of 1.15, the corresponding energy spread is corrected from 1.5% to 1.8%, as shown in Fig. 6(b).

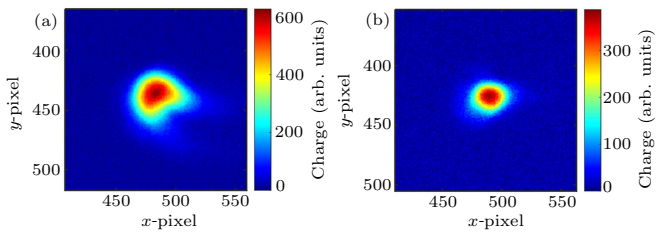


Fig. 6. Electron beam spot obtained on IP in experiment, with length-to-width radio k ($k = y_{\mathrm{FWHM}}/x_{\mathrm{FWHM}}$) being (a) 1.12, and (b) 1.15. The x and y coordinates denote the number of pixels in the corresponding directions, respectively, a total of 1024×1024. Color bar represents the number of electrons in each pixel.

In realistic conditions, there are multiple monoenergetic peaks as shown in the raw data for Fig. 6. To address this issue, we can draw inspiration from the variational autoencoder (VAE) in the field of machine learning, which decomposes the input waveform into a superposition of multiple Gaussian distributions.[26] The VAE is a neural network model that can map input data to a low-dimensional latent space, and the decoder maps the latent space vectors back to the original input space. By decoding the energy spectrum through using the Gaussian mixture model (GMM),[32] we can generate the corresponding means and variances of the Gaussian distributions and adjust the weights to achieve the best fitting effect.

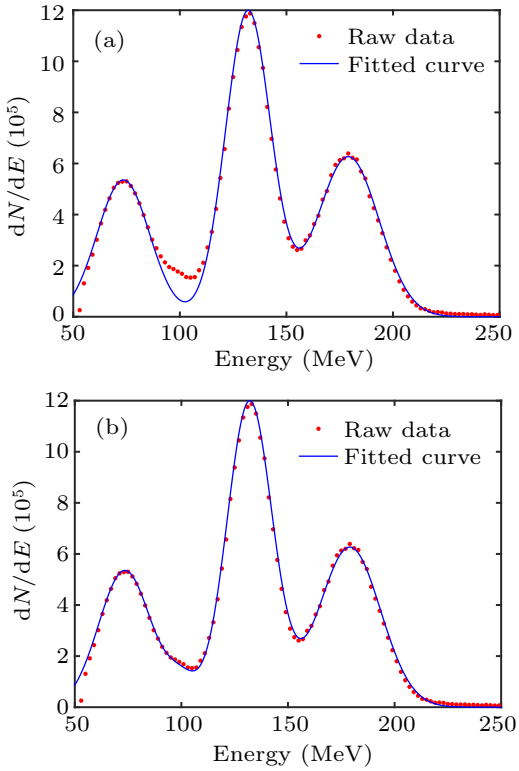


Fig. 7. (a) Fitting of three Gaussian functions mixed model and (b) four Gaussian functions mixed model.

The number of Gaussian distributions is set to 3 for the Gaussian mixture model algorithm based on the energy spectrum as shown in Fig. 7(a). However, the fit is not good near 100 MeV, suggesting the presence of a small electron beam. The fit is performed by using a four-component Gaussian mixture model as shown in Fig. 7(b), which works well. The algorithm can obtain the mean, variance (σ^2), and proportional weight, and this electron spectrum can be decomposed into four Gaussian distributions. This means that the Gaussian model used in the previous section can be adapted to general electron spectra. The corresponding distribution FWHM can be obtained using the property of Gaussian functions, that is, the relationship between FWHM and standard deviation (σ):

$$\mathrm{FWHM} = 2\sqrt{2\ln(2)}\sigma \approx 2.355\sigma.$$

5. Conclusion

In this work, we fill the gap in the study of energy spread measurements related to divergence angles by using numer-

ical simulations. The signification of considering the divergence angle in accurately measuring the energy spread of an electron beam is demonstrated by simulating 3×10^5 electrons with a central energy of 150 MeV and the divergence angle (3.5 mrad). The present work investigated the influence of the quasi-focusing property of the magnetic field produced by the C-shaped magnet on the electron beam spot. Specifically, the length-to-width ratio k of the electron beam spot is quantitatively analyzed as a function of the divergence angle, which grows exponentially with energy spread.

Our proposed method can effectively correct the energy spread of the electron beam. The modeling approach is a general method which can be applied to different experimental setups and configurations. For multi-electron spectra, the electron density profile can be decomposed into Gaussian distribution by GMM algorithm. This study provides support for precisely measuring high-quality electron bunch.

Data availability statement

The data that support the findings of this study are available from the corresponding authors according to reasonable requirements.

Acknowledgements

Project supported by the National Key Research and Development Program of China (Grant No. 2021YFA1601700), the National Natural Science Foundation of China (Grant Nos. 12074251, 11991073, 12335016, 12305272, and 12105174), the Strategic Priority Research Program of the Chinese Academy of Sciences (Grant Nos. XDA25000000 and XDA25030400), and Yangyang Development Fund, China.

References

[1] Esarey E, Schroeder C B and Leemans W P 2009 *Rev. Mod. Phys.* **81** 1229
[2] Di Mitri S and Cornacchia M 2014 *Phys. Rep.* **539** 1
[3] Wang W T, Li W T, Liu J S, Zhang Z J, Qi R, Yu C H, Liu J Q, Fang M, Qin Z Y, Wang C, Xu Y, Wu F X, Leng Y X, Li R X and Xu Z Z 2016 *Phys. Rev. Lett.* **117** 124801
[4] Faure J, Glinec Y, Pukhov A, Kiselev S, Gordienko S, Lefebvre E, Rousseau J P, Burgy F and Malka V 2004 *Nature* **431** 541
[5] Geddes C G R, Toth Cs, van Tilborg J, Esarey E, Schroeder C B, Bruhwiler D, Nieter C, Cary J and Leemans W P 2004 *Nature* **431** 538
[6] Mangles S P D, Murphy C D, Najmudin Z, Thomas A G R, Collier J L, Dangor A E, Divall E J, Foster P S, Gallacher J G, Hooker C J, Jaroszynski D A, Langley A J, Mori W B, Norreys P A, Tsung F S, Viskup R, Walton B R and Krushelnick K 2004 *Nature* **431** 535
[7] Zhu X, Li B, Liu F, Li J, Bi Z, Ge X, Deng H, Zhang Z, Cui P, Lu L, Yan W, Yuan X, Chen L, Cao Q, Liu Z, Sheng Z, Chen M and Zhang J 2023 *Phys. Rev. Lett.* **130** 215001
[8] Blumenfeld I, Clayton C E, Decker F J, Hogan M J, Huang C, Ischebeck R, Iverson R, Joshi C, Katsouleas T, Kirby N, Lu W, Marsh K A, Mori W B, Muggli P, Oz E, Siemann R H, Walz D and Zhou M 2007 *Nature* **445** 741
[9] Hue C S, Wan Y, Levine E Y and Malka V 2023 *Matter and Radiation at Extremes* **8** 024401
[10] Wang J, Zeng M, Li D, Wang X, Lu W and Gao J 2022 *Matter and Radiation at Extremes* **7** 054001
[11] Manahan G G, Habib A F, Scherkl P, Delinikolas P, Beaton A, Knetsch A, Karger O, Wittig G, Heinemann T, Sheng Z M, Cary J R, Bruhwiler D L, Rosenzweig J B and Hidding B 2017 *Nat. Commun.* **8** 15705
[12] Huang K, Jin Z, Nakanii N, Hosokai T and Kando M 2023 *Phys. Rev. Accel. Beams* **26** 112801
[13] Downer M C, Zgadzaj R, Debus A, Schramm U and Kaluza M C 2018 *Rev. Mod. Phys.* **90** 035002
[14] Pollock B B, Clayton C E, Ralph J E, Albert F, Davidson A, Divol L, Filip C, Glenzer S H, Herpoldt K, Lu W, Marsh K A, Meinecke J, Mori W B, Pak A, Rensink T C, Ross J S, Shaw J, Tynan G R, Joshi C and Froula D H 2011 *Phys. Rev. Lett.* **107** 045001
[15] Litos M, Adli E, An W, Clarke C I, Clayton C E, Corde S, Delahaye J P, England R J, Fisher A S, Frederico J, Gessner S, Green S Z, Hogan M J, Joshi C, Lu W, Marsh K A, Mori W B, Muggli P, Vafaei-Najafabadi N, Walz D, White G, Wu Z, Yakimenko V and Yocky G 2014 *Nature* **515** 92
[16] Yan W, Chen L, Li D, Zhang L, Hafz N A M, Dunn J, Ma Y, Huang K, Su L, Chen M, Sheng Z and Zhang J 2014 *Proc. Natl. Acad. Sci. USA* **111** 5825
[17] Mirzaie M, Li S, Zeng M, Hafz N A M, Chen M, Li G Y, Zhu Q J, Liao H, Sokollik T, Liu F, Ma Y Y, Chen L M, Sheng Z M and Zhang J 2015 *Sci. Rep.* **5** 14659
[18] Golovin G, Yan W, Luo J, Fruhling C, Haden D, Zhao B, Liu C, Chen M, Chen S, Zhang P, Banerjee S and Umstadter D 2018 *Phys. Rev. Lett.* **121** 104801
[19] Feng J, Li Y, Wang J, Li D, Li F, Yan W, Wang W and Chen L 2019 *Sci. Rep.* **9** 2531
[20] Jalas S, Kirchen M, Messner P, Winkler P, Hübner L, Dirkwinkel J, Schnepp M, Lehe R and Maier A R 2021 *Phys. Rev. Lett.* **126** 104801
[21] Ke L T, Feng K, Wang W T, Qin Z Y, Yu C H, Wu Y, Chen Y, Qi R, Zhang Z J, Xu Y, Yang X J, Leng Y X, Liu J S, Li R X and Xu Z Z 2021 *Phys. Rev. Lett.* **126** 214801
[22] Chen Q, Maslarova D, Wang J, Lee S X, Horný V and Umstadter D 2022 *Phys. Rev. Lett.* **128** 164801
[23] Rabhi N, Batani D, Boutoux G, Ducret J E, Jakubowska K, Lantuejoul-Thfoin I, Nauraye C, Patriarca A, Saïd A, Semsoum A, Serani L, Thomas B and Vauzour B 2017 *Rev. Sci. Instrum.* **88** 113301
[24] Singh S, Slavicek T, Hodak R, Versaci R, Pridal P and Kumar D 2017 *Rev. Sci. Instrum.* **88** 075105
[25] Wang T Y, Zhou Z Q, Peng J P, Gao Y K and Zhang Y H 2022 *Chin. Phys. B* **31** 076107
[26] Streeter M J V, Colgan C, Cobo C C, Arran C, Los E E, Watt R, Bourgeois N, Calvin L, Carderelli J, Cavanagh N, Dann S J D, Fitzgarrald R, Gerstmayr E, Joglekar A S, Kettle B, McKenna P, Murphy C D, Najmudin Z, Parsons P, Qian Q, Rajeev P P, Ridgers C P, Symes D R, Thomas A G R, Sarri G and Mangles S P D 2023 *High Power Laser Sci. Eng.* **11** 1
[27] Batygin Y K 2005 *Detectors and Associated Equipment* **539** 455
[28] Lund S M, Kikuchi T and Davidson R C 2009 *Phys. Rev. ST Accel. Beams* **12** 114801
[29] Lee S J R, Ding F, Manby F R and Miller T F 2019 *J. Chem. Phys.* **151** 064112
[30] Amarasinghe P A G M, Abeygunawardane S K and Singh C 2020 *IEEE Access* **8** 138661
[31] Brömmelhoff K, Henze S, Gerstenberger R, Fischer T, Schell N, Uhlmann E and Reimers W 2013 *Journal of Materials Processing Technology* **213** 2211
[32] Sun X, Yu Y, Yang Y, Dong J, Böhm C and Chen X 2020 *Chin. Phys. B* **29** 108901